Electronic Supplementary Information

Abiotic Reduction of 3-Nitro-1,2,4-triazol-5-one (NTO) and Other Munitions Constituents by Wood-Derived Biochar through Its Rechargeable Electron Storage Capacity

Danhui Xin[†], Julián Girón[†], Mark E. Fuller[‡], and Pei C. Chiu[†]*

[†]Department of Civil & Environmental Engineering, University of Delaware, Newark, DE 19716, USA

[‡]Aptim Federal Services, 17 Princess Road, Lawrenceville, NJ 08648, USA

[*]**Corresponding Author**

Pei C. Chiu, Department of Civil and Environmental Engineering, University of Delaware, Newark, DE 19716; Email: pei@udel.edu; https://orcid.org/0000-0003-2319-4496

This Electronic Supplementary Information contains **23 pages, 6 sections, 7 tables, and 10 figures**.

Contents

Sections:

Tables:

Figures:

Table S1. List of chemicals used [a]

	Name	Formula	Purity	Manufacturer
Buffer	2-(N-morpholino)ethanesulfonic acid (MES)	$C_6H_{13}NO_4S$	>98%	Fisher Scientific (Pittsburgh, PA)
	2-amino-2-(hydroxymethyl)-1,3-propanediol (Tris, base)	$C_4H_{11}NO_3$	99.8%	Sigma-Aldrich (St. Louis, MO)
	3-(cyclohexylamino)-2-hydroxy-1-propanesulfonic acid (CAPSO)	$C_9H_{19}NO_4S$	>99%	Acros Organics (Morris Plains, NJ)
	2-[4-(2-hydroxyethyl)piperazin-1-yl]ethanesulfonic acid (HEPES)	$C_8H_{17}N_2NaO_4S$	>99%	Fisher Scientific
Artificial stormwater runoff (ASR)	sodium chloride	NaCl	99%	Fisher Scientific
	potassium chloride	KCl	99+%	Acros Organics
	magnesium chloride hexahydrate	$MgCl_2 \cdot 6H_2O$	99%	Fisher Scientific
	calcium chloride dihydrate	$CaCl_2 \cdot 2H_2O$	98+%	Fisher Scientific
	sodium sulfate anhydrous	Na_2SO_4	99.8%	Fisher Scientific
	ammonium sulfate	$(NH_4)_2SO_4$	99%	Fisher Scientific
	calcium nitrate tetrahydrate	$Ca(NO_3)_2 \cdot 4H_2O$	>99%	Fisher Scientific
pH control	hydrochloric acid solution	HCl	37.2% (ACS plus)	Fisher Scientific
	sodium hydroxide solution	NaOH	1N standard solution (trace metal grade)	Acros Organics

Eluents for HPLC	acetonitrile	C_2H_3N	>99.9%	Fisher Scientific
	trifluoroacetic acid	$C_2HF_3O_2$	>99.9%	MilliporeSigma (Burlington, MA)
	methanol	CH_3OH	>99.9%	Fisher Scientific
	potassium phosphate dibasic	K_2HPO_4	99.4%	Fisher Scientific
	potassium phosphate monobasic	KH_2PO_4	99.5%	J.T. Baker (Phillipsburg, NJ)
Redox titrants	sodium dithionite	$Na_2S_2O_4$	>85%	Alfa Aesar (Haverhill, MA)
	potassium ferricyanide	$K_3Fe(CN)_6$	>99%	Acros Organics

[a] Information on MCs is provided in the main text.

Section S1. Biochar characterization

The properties of the biochar we measured include elemental composition (CHNS), ash content, pH, BET surface area, cation exchange capacity (CEC), and ESC. Prior to characterization, each biochar was sieved to obtain a size fraction of 250–500 μm, washed with deionized water thoroughly, dried at 65 °C for 24 h, and stored in a desiccator.

Carbon, hydrogen, nitrogen, sulfur contents were determined using a vario MACRO cube (Elementar, Langenselbold, Germany). Fully dried samples (5-20 mg) were combusted at *ca*. 960 °C in ultra-high-purity oxygen, and passed through copper oxide pellets and then electrolytic copper with helium as carrier gas. The gases were quantified by a thermal conductivity detector (TCD). The oxygen content was estimated by subtracting carbon, hydrogen, nitrogen, sulfur, and ash contents from 100%. Ash contents were measured by combusting a biochar sample (5-10 mg) in air at 900 °C for 5 min using a Discovery thermogravimetric analyzer (TA Instruments, New Castle, DE). Ash contents were taken to be the mass remaining after combustion.

For pH measurement, 0.5 g of biochar was placed in 10 mL of deionized water (1:20 w/v) and equilibrated for 24 h. Solution pH was measured using an Oakton 11 series pH/mV/°C meter and an Oakton pH electrode (Vernon Hills, IL), calibrated against pH 4, 7, and 10 standards. The specific surface area was measured using a Micromeritics BET surface area analyzer (Norcross, GA) through N_2 adsorption to a biochar sample of known mass at 77.382 K. CEC was measured by NH_4^+ replacement using EPA Method 9080. NH_4^+ concentration was determined using a Metrohm 850 Professional IC AnCat unit equipped with a conductivity detector (Herisau, Switzerland). ESC was measured in our previous study through chemical redox titration[1,2] using dissolved oxygen (DO, +0.80 V vs. SHE at pH 7, P_{O_2}= 0.21 atm) and titanium(III) citrate (–0.36 V vs. SHE at pH 6.4) as oxidant and reductant, respectively. A portion of the electrons stored in dithionite-reduced biochar was retrieved using 10 mM ferricyanide in 20 mM phosphate buffer according to the method we previously published.[2]

Table S2. Physical-chemical properties of biochars

		Soil Reef biochar (SRB)	Rogue biochar (Rogue)
Vendor		The Biochar Company [a]	Oregon Biochar Solutions
Source material		Southern Yellow Pine	Douglas Fir + Ponderosa Pine
Pyrolysis temperature (°C)		550 (slow pyrolysis)	900 (fast pyrolysis)
Elemental composition (%)	C	72.01±5.00	68.47±10.00
	H	1.96±0.02	1.50±0.20
	N	0.36±0.08	0.28±0.07
	S	0.26±0.03	0.24±0.15
	O	20.82±5.00	16.99±10.00
Ash (%)		4.59±1.30	12.52±0.50
pH		7.53±0.05	8.88±0.08
BET (m^2/g)		158±3	407±9
CEC [a] (mmol/g)		0.42±0.02	0.12±0.03
ESC (mmol/g) measured with Ti(III) citrate and DO		3.54±0.13 (2.43±0.00) [b]	7.07±0.15 (6.78±0.20) [b]

Errors represent the range of results from duplicates.

[a] CEC measured using EPA Method 9080.

[b] Regenerable ESC, measured over two additional redox cycles.

Table S3. Summary of batch reaction conditions for MC reduction

	MC	C_{aq0}	Biochar	Dose	pH	Background solution	Replicates	Figure
Buffered system	NTO	110 μM	SRB_{OX}, SRB_{RED}	0.80 g/L	6	50mM MES	3	1(a)
	NTO	110 μM	SRB_{OX}, SRB_{RED}	0.80 g/L	8	50mM Tris	3	1(b)
	NTO	110 μM	SRB_{OX}, SRB_{RED}	0.80 g/L	10	50mM CAPSO	3	1(c), 2(a)
	NTO	110 μM	SRB_{OX}, SRB_{RED}	0.40 g/L	10	50mM CAPSO	3	2(b)
	ATO	120 μM	SRB_{RED}	0.80 g/L	6, 8, and 10 [a]		2	S2
	NQ	100 μM	SRB_{RED}	1.33 g/L	6 and 8 [a]		2	S6(b)
	NQ	100 μM	SRB_{OX}, SRB_{RED}	1.33 g/L	8	50mM Tris	2	S8
ASR	NTO	110 μM	SRB_{OX}, SRB_{RED}	0.80 g/L	6	ASR	3	6(a), (b)
	NTO	110 μM	$Rogue_{OX}$, $Rogue_{RED}$	0.80 g/L	6	ASR	3	6(a), (b)
	DNAN	400 μM	$Rogue_{OX}$, $Rogue_{RED}$	0.44 g/L	6	ASR	2	6(c), (d)
	RDX	200 μM	$Rogue_{OX}$, $Rogue_{RED}$	0.44 g/L	6	ASR	2	6(e), (f)
	2ANAN	350 μM	$Rogue_{OX}$, $Rogue_{RED}$	0.44 g/L	6	ASR	2	S9(a)
	NO_2^-	200 μM	$Rogue_{OX}$, $Rogue_{RED}$	0.44 g/L	6	ASR	2	S9(b)

All experiments were run in an anaerobic glove box.

[a] 50 mM MES, Tris, and CAPSO buffers were used, respectively, to control the pH at 6, 8, and 10.

Table S4. Summary of batch reaction conditions for MC sorption

MC	C_{aq0}	Biochar	Dose	pH	Background solution	Replicates	Figure
NTO	5-125 µM	$Rogue_{OX}$	0.20 g/L	6	ASR	2	5(a), S5(a)
NQ	20-250 µM	$Rogue_{OX}$	0.44 g/L	6	ASR	2	5(b), S5(b)
DNAN	30-300 µM	$Rogue_{OX}$	0.33 g/L	6	ASR	2	5(c), S5(c)
RDX	10-125 µM	$Rogue_{OX}$	0.88 g/L	6	ASR	2	5(d), S5(d)
NQ	200 µM	SRB_{OX}	0.80 g/L	8	50mM Tris	2	S6(a)
NQ	25-200 µM	SRB_{OX}	0.80 g/L	8	50mM Tris	2	S7(a), (b)

All experiments were run outside of an anaerobic glove box.

Section S2. The pK_a of ATO

Since an experimentally measured pK_a was not available for ATO in the literature, we performed a titration using NaOH to determine the pK_a of ATO. As 10 mM NaOH solution was added drop by drop to 25 mL of 10 mM ATO in 100 mM KCl, the volume of NaOH added and the pH were recorded. For the titration of ATO (a weak acid) with NaOH (a strong base), we applied the Gran method to obtain the pK_a of ATO. Based on the Gran plot shown in Figure S1, the K_a of ATO = $1.95\times10^{-9}\pm6\times10^{-11}$, obtained through linear regression of data before the equivalence point. This corresponds to a pK_a of **8.71±0.02**.

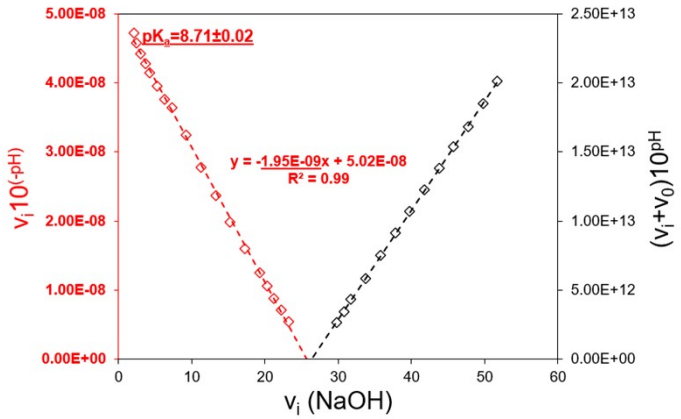

Figure S1. Gran plot for ATO titration with NaOH. The X axis is the total volume of NaOH (v_i) added to the ATO solution up to the ith point. The left and right Y axes are calculated values of v_i10^{-pH} and $(v_i+v_0)10^{pH}$, respectively, where v_0 is the initial ATO solution volume. Titration data before and after the equivalence point are plotted in red diamonds on the left Y axis and in black diamonds on the right Y axis, respectively.

Below is a description of the Gran method[3]:

At any point:

$$K_a = \frac{[H^+]_i[ATO^-]_i}{[HATO]_i} \qquad \text{[Eq. S1]}$$

where HATO and ATO^- represent the protonated and deprotonated forms of ATO, respectively.

Before the equivalence point, approximations below can be made:

$$[HATO]_i \approx \frac{v_0[HATO]_0 - v_i[OH^-]_0}{v_0 + v_i} \qquad \text{[Eq. S2]}$$

$$[ATO^-]_i \approx \frac{v_i[OH^-]_0}{v_0 + v_i} \quad \text{[Eq. S3]}$$

where v_0 and v_i are the initial ATO solution volume (25 mL) and total volume of added NaOH up to the ith point, respectively; $[HATO]_0$ is the initial ATO concentration (10 mM), and $[OH^-]_0$ is the concentration of the titrant (10 mM).

Substituting Eq. S2 and Eq. S3 for $[HATO]_i$ and $[ATO^-]_i$ in Eq. S1, respectively, yields:

$$K_a \approx \frac{[H^+]_i v_i [OH^-]_0}{v_0[HATO]_0 - v_i[OH^-]_0} \quad \text{[Eq. S4]}$$

and

$$[H^+]_i v_i = 10^{-pH_i} v_i \approx -K_a\left(v_i - v_0\frac{[HATO]_0}{[OH^-]_0}\right) \quad \text{[Eq. S5]}$$

Therefore, before the equivalence point, if $10^{-pH_i}v_i$ is plotted against v_i, the slope is $-K_a$ and the equivalence point (X intercept) is $v_0\frac{[HATO]_0}{[OH^-]_0}$.

At any point:

$$[OH^-]_i \approx \frac{v_i[OH^-]_0 - v_0[HATO]_0}{v_0 + v_i} \quad \text{[Eq. S6]}$$

and

$$\frac{[OH^-]_i(v_0 + v_i)}{K_w} = 10^{pH_i}(v_0 + v_i) \approx \frac{[OH^-]_0}{K_w}\left(v_i - v_0\frac{[HATO]_0}{[OH^-]_0}\right) \quad \text{[Eq. S7]}$$

After the equivalence point, when $10^{pH_i}(v_0 + v_i)$ is plotted against v_i, the equivalence point is $v_0\frac{[HATO]_0}{[OH^-]_0}$, meaning the two curves would have the same X intercept.

Section S3. ATO sorption to SRB_{RED}

0.80 g/L of SRB_{RED} was added to reactors containing ATO to determine the sorption of ATO to SRB_{RED} at different pH. As shown in Figure S2, the amount of ATO sorbed to SRB_{RED} at the end of the experiment was 12±5 and 17±2 µmol/g at pH 6 and 8, respectively. In contrast, the sorption of ATO to SRB_{RED} was negligible at pH 10.

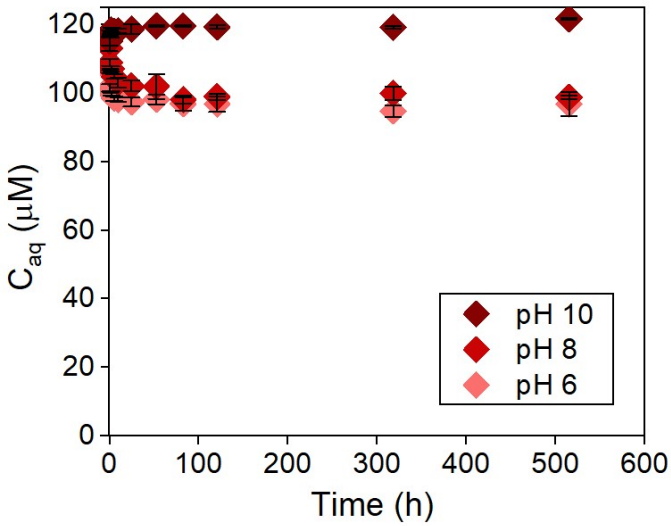

Figure S2. Sorption of ATO to 0.80 g/L of SRB_{RED} at pH 6, 8, and 10.

Table S5. Mass balance of NTO reduction by biochar in buffered solutions

Figure 1(a): pH 6 in 50 mM MES buffer				
Biochar	SRB_{OX}		SRB_{RED}	
Dose	0.80 g/L		0.80 g/L	
(μmol/g)	average	stdev	average	stdev
NTO_{total}	138	0	138	0
NTO_{aq}	114	2	26	8
ATO_{aq}	–	–	86	5
NTO_s	16	2	0	0
ATO_s	–	–	14	2
Mass balance (%)	94±3%		91±10%	
NTO_{total}–NTO_{aq} (μmol/g)	24±0		112±8	
ATO_{total} (μmol/g)	–		100±7	

Figure 1(b): pH 8 in 50 mM Tris buffer				
Biochar	SRB_{OX}		SRB_{RED}	
Dose	0.80 g/L		0.80 g/L	
(μmol/g)	average	stdev	average	stdev
NTO_{total}	134	0	134	0
NTO_{aq}	124	0	40	7
ATO_{aq}	–	–	68	6
NTO_s	11	0	0	0
ATO_s	–	–	14	2
Mass balance (%)	101±0%		91±12%	
NTO_{total}–NTO_{aq} (μmol/g)	10±0		94±7	
ATO_{total} (μmol/g)			82±8	

Figures 1(c) and 2(a and b): pH 10 in 50 mM CAPSO buffer								
Biochar	SRB_{OX}				SRB_{RED}			
Dose	0.80 g/L		0.40 g/L		0.80 g/L		0.40 g/L	
(μmol/g)	average	stdev	average	stdev	average	stdev	average	stdev
NTO_{total}	129	0	258	1	129	0	258	1
NTO_{aq}	127	0	255	1	45	8	172	12

ATO_{aq}	–	–	–	–	84	4	86	12
NTO_s	–	–	–	–	–	–	–	–
ATO_s	–	–	–	–	–	–	–	–
Mass balance (%)	98±0%		99±0%		100±9%		101±10%	
NTO_{total}–NTO_{aq} (μmol/g)	2±0		3±0		84±8		86±13	
ATO_{total} (μmol/g)					84±4		86±12	

Section S4. Thermodynamic calculation for the redox reaction between a model hydroquinone (AH_2QDS) and ferricyanide

To elucidate the pH dependency of the redox reaction between SRB_{RED} and ferricyanide, we use 9,10-anthrahydroquinone-2,6-disulfonate (AH_2QDS) as a hypothetical hydroquinone in SRB_{RED} to calculate how the thermodynamic driving force for the redox reaction can vary with pH.

Since no H^+ is involved, reduction of ferricyanide is pH-independent and can be described by the following half-reaction (Eq. S8):

$$Fe(CN)_6^{3-} + e^- \rightarrow Fe(CN)_6^{4-} \quad \text{[Eq. S8]}$$

Because the first pK_a of AH_2QDS is 7.6[4], reduction of AQDS, the oxidized counterpart of AH_2QDS, can be described by the following half-reactions (Eqs. S9a, b).

$$AQDS + 2\,H^+ + 2\,e^- \rightarrow AH_2QDS\ (pH<7.6) \quad \text{[Eq. S9a]}$$

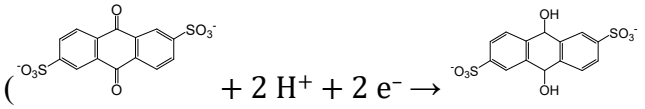

[Eq. S9a])

$$AQDS + H^+ + 2\,e^- \rightarrow AHQDS^-\ (pH>7.6) \quad \text{[Eq. S9b]}$$

where AH_2QDS and $AHQDS^-$ represent the fully protonated and singly deprotonated forms of AH_2QDS.

Midpoint reduction potential ($E_H^{'}$)[5] represents the reduction potential of a half-reaction at which the total concentration of all the oxidized species is equal to that of all the reduced species, as shown in Eqs. S10 and S11.

$$[Fe(CN)_6^{3-}] = [Fe(CN)_6^{4-}] \quad \text{[Eq. S10]}$$

$$[AQDS] = [AH_2QDS] + [AHQDS^-] \quad \text{[Eq. S11]}$$

At any given pH, the midpoint reduction potential of the half-reaction Eq. S8 can be obtained from the Nernst equation and Eq. S10:

$$E_{H(Fe(CN)_6^{3-}/Fe(CN)_6^{4-})}^{'} = E_{H(Fe(CN)_6^{3-}/Fe(CN)_6^{4-})}^{0} \quad \text{[Eq. S12]}$$

where the standard reduction potential $E_{H(Fe(CN)_6^{3-}/Fe(CN)_6^{4-})}^{0}$ is +0.43 V[6].

Likewise, the midpoint reduction potential of the half-reaction Eq. S9 can be obtained from the Nernst equation and Eq. S11:

$$E_{H(AQDS/AH_2QDS)}^{'} = E_{H(AQDS/AH_2QDS)}^{0} + 2.303\frac{RT}{2F}\log\left([H^+]^2 + K_{a,\,AH_2QDS}[H^+]\right) \quad \text{[Eq. S13]}$$

where $E^0_{H(AQDS/AH_2QDS)}$ is +0.23 V[4] at pH 0 and K_{a,AH_2QDS} is 7.6[4].

Therefore, the ΔE^0_H of the redox reaction between ferricyanide and AH_2QDS can be calculated by Eq. S14:

$$\Delta E'_{H(Fe(CN)_6^{3-}/AH_2QDS)} = E'_{H(Fe(CN)_6^{3-}/Fe(CN)_6^{4-})} - E'_{H(AQDS/AH_2QDS)} \quad \text{[Eq. S14]}$$

As illustrated in Figure S3, the driving force ($\Delta E'_H$) for the reduction of hydroquinone (and presumably reduced biochar) by ferricyanide *increases with pH* as hydroquinone deprotonates (see the star-shaped data points in Figure 3).

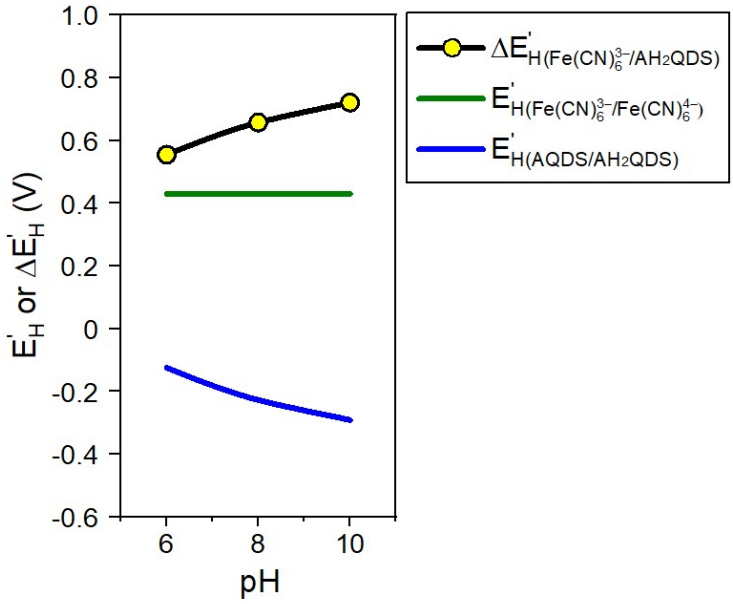

Figure S3. $E'_H - pH$ diagram. $E'_{H(Fe(CN)_6^{3-}/Fe(CN)_6^{4-})}$, $E'_{H(AQDS/AH_2QDS)}$, and $\Delta E'_{H(Fe(CN)_6^{3-}/AH_2QDS)}$ were calculated based on Eqs. S12, S13, and S14, respectively.

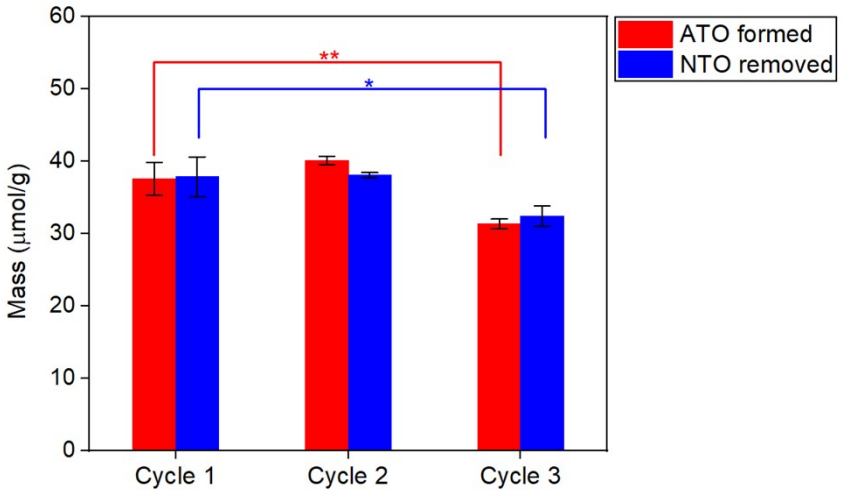

Figure S4. The amounts of NTO removed and ATO produced with the same 0.80 g/L of SRB_{RED} ("ESC-recharged") at pH 10 over three consecutive redox cycles. SRB_{RED} was regenerated with dithionite between two consecutive cycles. Single (*) and double (**) asterisks denote differences between cycle 1 and cycles 2 and 3 using a student's t-test on a significance level of 0.05 and 0.01 (i.e., $p<0.05$ and $p<0.01$), respectively.

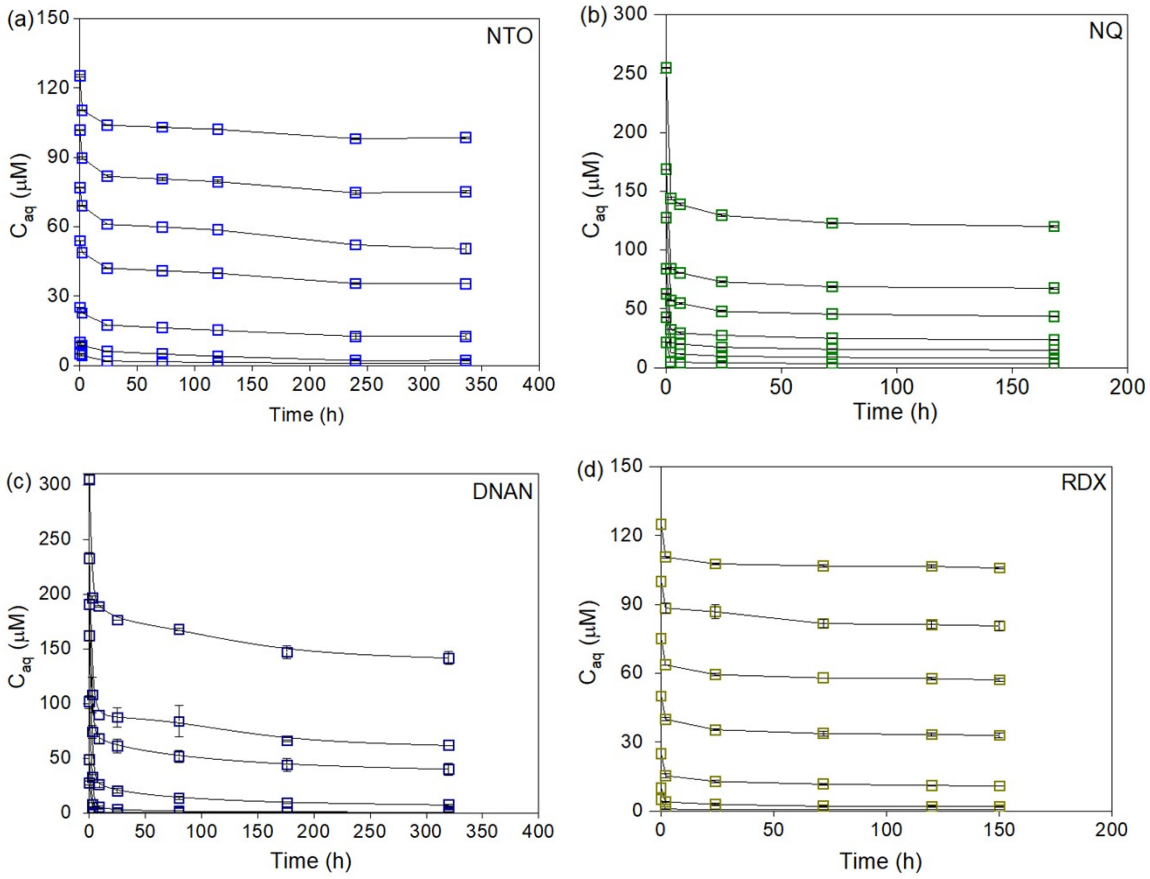

Figure S5. Sorption of MCs to $Rogue_{OX}$ over time. Experiments were performed in ASR at pH 6 with different initial MC concentrations. (a) NTO to 0.20 g/L $Rogue_{OX}$ (b) NQ to 0.44 g/L $Rogue_{OX}$ (c) DNAN to 0.33 g/L $Rogue_{OX}$ (d) RDX to 0.88 g/L $Rogue_{OX}$

Table S6. Extraction efficiency of sorbed MCs from $Rogue_{OX}$. $Rogue_{OX}$ samples that sorbed the maximum amount of each MC in Figure S5 were subjected to solvent extractions to obtain these extraction efficiencies.

	Removal (µmol/g)		Recovery (µmol/g)		Extraction efficiency (%)
	average	stdev	average	stdev	
NTO	133	4	110	2	83±1%
NQ	374	0	329	32	88±8%
DNAN	477	8	421	17	88±4%
RDX	214	3	180	12	84±6%

Section S5. NQ sorption to biochar

Parallel sorption experiments for NQ were first conducted inside and outside of the glovebox. The results in Figure S6(a) confirmed that the sorption of NQ is not influenced by the atmosphere. Thus, all other sorption experiments were conducted outside of an anaerobic glovebox. As NQ is a neutral compound under circumneutral pH conditions, a similar amount of NQ was removed at pH 6 and 8 (Figure S6(b)). We chose pH 8 to further assess the sorption of NQ to SRB for obtaining its Langmuir isotherm (Figure S7).

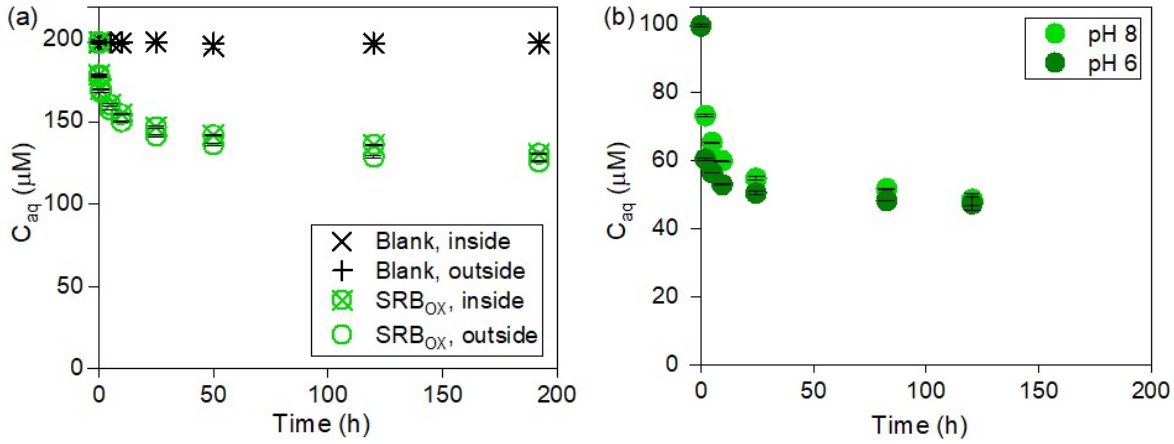

Figure S6. (a) Sorption of NQ to 0.80 g/L of SRB_{OX} inside vs. outside of the glovebox in 50 mM Tris buffer at pH 8. (b) Sorption of NQ to 1.33 g/L of SRB_{RED} at pH 6 (50 mM MES buffer) vs. pH 8 (50 mM Tris buffer) in the glovebox.

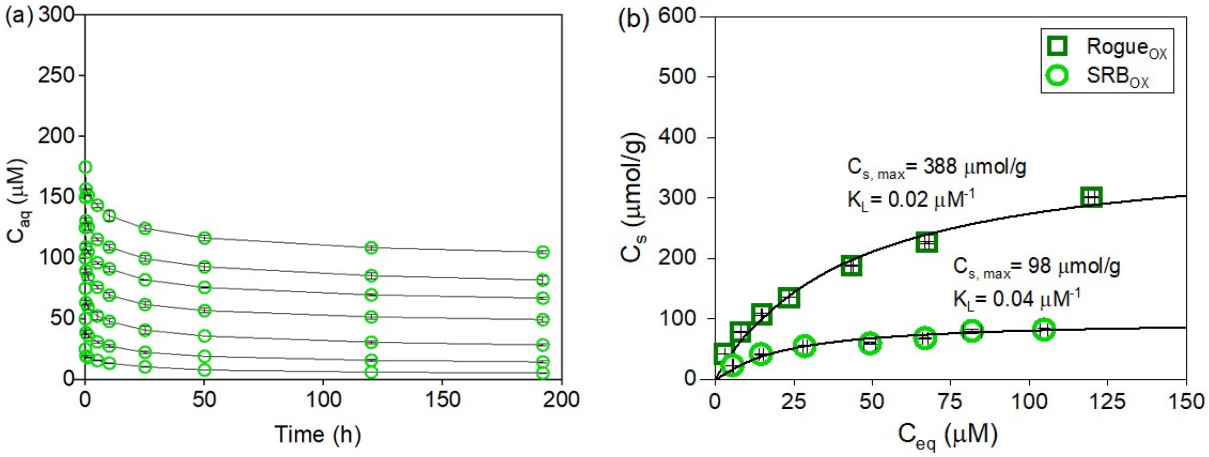

Figure S7. (a) Sorption of NQ to 0.80 g/L of SRB_{OX} at pH 8. (b) Comparison of NQ sorption to 0.80 g/L SRB_{OX} in 50 mM Tris buffer at pH 8 and to 0.44 g/L of $Rogue_{OX}$ in ASR at pH 6, and

their fitted Langmuir isotherms. The regression R^2 of the measured and predicted sorption capacities of SRB_{OX} and of $Rogue_{OX}$ for NQ based on the fitted Langmuir isotherms were 0.98 and 0.96, respectively.

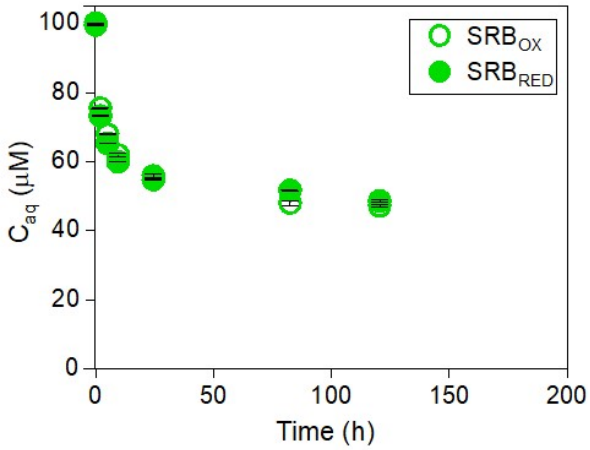

Figure S8. Aqueous concentration (C_{aq}) of NQ over time with 1.33 g/L of SRB_{OX} or SRB_{RED} at pH 8.

Table S7. Mass balance of MC reduction by biochar in ASR at pH 6

		SRB_{OX}		SRB_{RED}	
Figures 6(a) and (b): NTO	(µmol/g)	average	stdev	average	stdev
	NTO_{total}	135	2	135	2
	NTO_{aq}	120	1	32	7
	ATO_{aq}	–	–	77	5
	NTO_s	16	0	1	1
	ATO_s	–	–	14	5
	Mass balance (%)	100±1%		94±4%	
	NTO_{total}–NTO_{aq} (µmol/g)	15±2		103±8	
	ATO_{total} (µmol/g)	–		91±6	
		$Rogue_{OX}$		$Rogue_{RED}$	
	(µmol/g)	average	stdev	average	stdev
	NTO_{total}	138	0	138	0
	NTO_{aq}	94	5	26	2
	ATO_{aq}	–	–	73	1
	NTO_s	29	2	2	0
	ATO_s	–	–	21	1
	Mass balance (%)	88±5%		89±3%	
	NTO_{total}–NTO_{aq} (µmol/g)	44±6		112±2	
	ATO_{total} (µmol/g)	–		94±2	
Figures 6(c) and (d): DNAN		$Rogue_{OX}$		$Rogue_{RED}$	
	(µmol/g)	average	stdev	average	stdev
	$DNAN_{total}$	911	5	911	5
	$DNAN_{aq}$	397	11	281	30
	$2ANAN_{aq}$	–	–	24	3
	$4ANAN_{aq}$	–	–	1	0
	$DNAN_s$	444	15	454	30
	$2ANAN_s$	–	–	42	11
	$4ANAN_s$	–	–	1	1
	Mass balance (%)	92±3%		88±9%	

	$DNAN_{total}$-$DNAN_{aq}$ (µmol/g)	518±5		630±20	
	$2ANAN_{total}$+$4ANAN_{total}$ (µmol/g)	–		67±7	
Figures 6(e) and (f): RDX		$Rogue_{OX}$		$Rogue_{RED}$	
	(µmol/g)	average	stdev	average	stdev
	RDX_{total}	452	20	434	20
	RDX_{aq}	220	2	102	6
	MNX_{aq}	–	–	2	0
	$NO_2^-{}_{aq}$	–	–	9	6
	RDX_s	212	11	162	11
	MNX_s	–	–	3	0
	Mass balance (%)	96±3%		64±4%	
	RDX_{total}–RDX_{aq} (µmol/g)	232±20		332±19	
	MNX_{total}+$NO_2^-{}_{total}$ (µmol/g)	–		14±6	

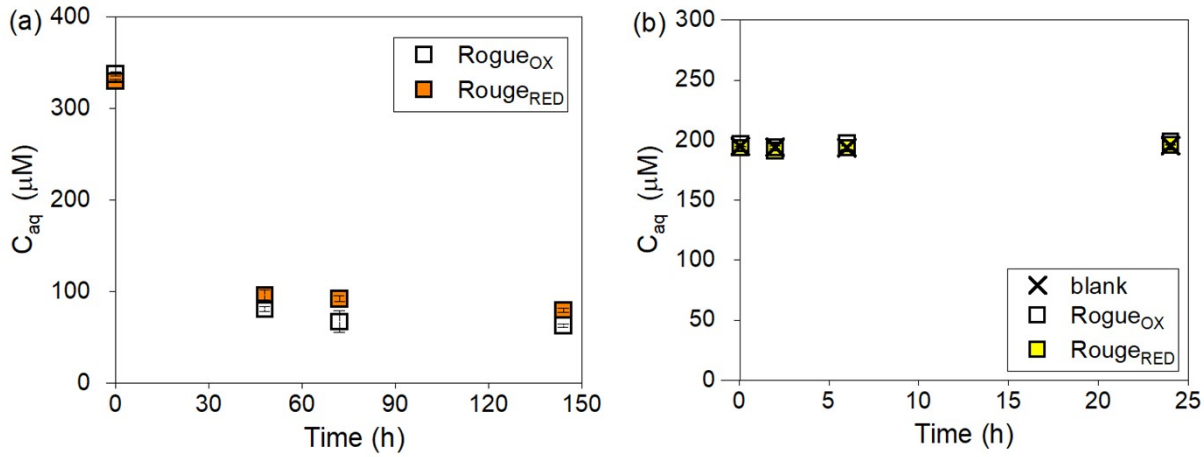

Figure S9. Aqueous concentration (C_{aq}) of the daughter product of MC transformation over time with 0.44 g/L of Rogue in ASR at pH 6. (a) 2ANAN (b) NO_2^-

Section S6. NO_2^- production from the abiotic transformation of RDX by $Rogue_{RED}$

To verify the production of NO_2^- from the abiotic reduction of RDX by $Rogue_{RED}$, batch reactors containing 1 g of either $Rogue_{OX}$ or $Rogue_{RED}$ were prepared in duplicates. Each reactor contained 0.2 L of *ca.* 140 µM RDX (corresponding to 28 µmol of RDX). Solutions were buffered with 25 mM HEPES at pH 7 instead of ASR because the Cl^- in ASR interfered with ion chromatographic (IC) detection of NO_2^-. Due to the low solubility of RDX (270 µM[7]), four additional aliquots of RDX stock solution (6 mL per aliquot, each containing 9.32 µmol RDX) were added to the reactor at later times. NO_2^- was measured using a Metrohm 850 Professional IC.

As shown in Figure S10, in contrast to reactors containing $Rogue_{OX}$ where no NO_2^- was detected, about 5.5 µmol of NO_2^- was produced within 1 h. As more RDX was added in four additional doses, 6 and 7 µmol of NO_2^- were formed after the first and second doses, respectively, while further NO_2^- formation was minimal following the third and fourth doses. The total amount of NO_2^- produced per gram of $Rogue_{RED}$ was 22 µmol, clearly indicating the ESC of Rogue was accessible to and reactive toward RDX.

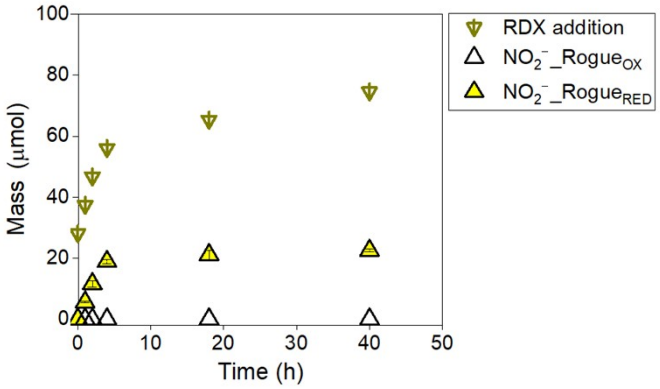

Figure S10. NO_2^- formation upon RDX addition to reactors containing 5 g/L of Rogue.

References

1. D. Xin, N. Saha, M. T. Reza, J. Hudson and P. C. Chiu, Pyrolysis creates electron storage capacity of black carbon (biochar) from lignocellulosic biomass, *ACS Sustainable Chemistry & Engineering*, 2021 **9**, 6821-6831. 10.1021/acssuschemeng.1c01251
2. D. Xin, M. Xian and P. C. Chiu, New methods for assessing electron storage capacity and redox reversibility of biochar, *Chemosphere*, 2019, **215**, 827-834. 10.1016/j.chemosphere.2018.10.080
3. G. Gran, Determination of the equivalence point in potentiometric titrations. Part II, *Analyst*, 1952, **77**, 661-671. 10.1039/AN9527700661
4. J. Murillo-Gelvez, K. P. Hickey, D. M. Di Toro, H. E. Allen, R. F. Carbonaro and P. C. Chiu, Experimental validation of hydrogen atom transfer Gibbs free energy as a predictor of nitroaromatic reduction rate constants, *Environmental Science & Technology*, 2019, **53**, 5816-5827. 10.1021/acs.est.9b00910
5. W. M. Clark, Oxidation-reduction potentials of organic systems, 1960.
6. M. Aeschbacher, M. Sander and R. P. Schwarzenbach, Novel electrochemical approach to assess the redox properties of humic substances, *Environmental Science & Technology*, 2010, **44**, 87-93. 10.1021/es902627p
7. K. Dontsova, S. Taylor and R. Pesce-Rodriguez, *SERDP Project ER-2220: Dissolution of NTO, DNAN and insensitive munitions formulations and their fates in soils*, University of Arizona, Tuscon, United States, February 2018.